Intrinsic quality factor determination in whispering gallery mode microcavities using a single Stokes parameters measurement

Francis Vanier,* Cecilia La Mela, Ahmad Hayat, and Yves-Alain Peter

Microphotonics Laboratory, Department of Engineering Physics,
École Polytechnique de Montréal
P.O. Box 6079, Station Centre-Ville, Montréal (QC), H3C 3A7 CANADA

*francis-2.vanier@polymtl.ca

http://www.polymtl.ca/pomp/en/

Abstract: Determination of the intrinsic quality factor of a loaded whispering gallery mode microcavity can be important for many applications where the coupling conditions cannot be tuned. We propose a single-scan technique based on a Stokes parameters analysis to extract the intrinsic quality factor and therefore determine the coupling regime. We propose a simple model for this analysis and present experimental measurements, which are in very good agreement with the model.

© 2011 Optical Society of America

OCIS codes: (140.3945) Microcavities; (130.5440) Polarization-selective devices; (260.5430) Polarization.

References and links

1. F. Vollmer and S. Arnold, "Whispering-gallery-mode biosensing: label-free detection down to single molecules," Nat. Methods **5**, 591–596 (2008).
2. J. Zhu, S. K. Ozdemir, Y. F. Xiao, L. Li, L. He, D.-R. Chen, and L. Yang, "On-chip single nanoparticle detection and sizing by mode splitting in an ultrahigh-Q microresonator," Nat. Photonics **4**, 46–49 (2009).
3. A. A. Savchenkov, V. S. Ilchenko, A. B. Matsko, and L. Maleki, "Kilohertz optical resonances in dielectric crystal cavities," Phys. Rev. A **70**, 051804(R) (2004).
4. S. L. McCall, A. F. J. Levi, R. E. Slusher, S. J. Pearton, and R. A. Logan, "Whispering-gallery mode microdisk lasers," Appl. Phys. Lett. **60**, 289–291 (1992).
5. T. J. Kippenberg, H. Rokhsari, T. Carmon, A. Scherer, and K. J. Vahala, "Analysis of radiation-pressure induced mechanical oscillation of an optical microcavity," Phys. Rev. Lett. **95**, 033901 (2005).
6. V. R. Almeida, C. A. Barrios, R. R. Panepucci, and M. Lipson, "All-optical control of light on a silicon chip," Nature **431**, 1081–1084 (2004).
7. M. L. Gorodetsky, A. A. Savchenkov, and V. S. Ilchenko, "Ultimate Q of optical microsphere resonators," Opt. Lett. **21**, 453–455 (1996).
8. D. K. Armani, T. J. Kippenberg, S. M. Spillane, and K. J. Vahala, "Ultra-high-Q toroid microcavity on a chip," Nature **421**, 925–928 (2003).
9. B. E. Little, J. S. Foresi, G. Steinmeyer, E. R. Thoen, S. T. Chu, H. A. Haus, E. P. Ippen, L. C. Kimerling, and W. Greene, "Ultra-compact Si-SiO_2 microring resonator optical channel dropping filters," IEEE Photonics Technol. Lett. **10**, 549–551 (1998).
10. M. Sumetsky, "Optimization of optical ring resonator devices for sensing applications," Opt. Lett. **32**, 2577–2579 (2007).
11. M. Hossein-Zadeh and K. J. Vahala, "Importance of intrinsic-Q in microring-based optical filters and dispersion-compensation devices," IEEE Photonics Technol. Lett. **19**, 1045–1047 (2007).
12. S. M. Spillane, T. J. Kippenberg, O. J. Painter, and K. J. Vahala, "Ideality in a fiber-taper-coupled microresonator system for application to cavity quantum electrodynamics," Phys. Rev. Lett. **91**, 043902 (2003).

#154353 - $15.00 USD Received 12 Sep 2011; revised 13 Oct 2011; accepted 16 Oct 2011; published 3 Nov 2011
(C) 2011 OSA

13. B. J. J. Slagmolen, M. B. Gray, K. G. Baigent, and D. E. McClelland, "Phase-sensitive reflection technique for characterization of a Fabry-Perot interferometer," Appl. Opt. **39**, 3638–3643 (2000).
14. C. R. Locke, D. Stuart, E. N. Ivanov, and A. N. Luiten, "A simple technique for accurate and complete characterisation of a Fabry-Perot cavity," Opt. Express **17**, 21935–21943 (2009).
15. Y. Dumeige, S. Trebaol, L. Ghişa, T. K. N. Nguyên, H. Tavernier, and P. Féron, "Determination of coupling regime of high-Q resonators and optical gain of highly selective amplifiers," J. Opt. Soc. Am. B **25**, 2073–2080 (2008).
16. T. Ito and Y. Kokubun, "Nondestructive measurement of propagation loss and coupling efficiency in microring resonator filters using filter responses," Jpn. J. Appl. Phys. **43**, 1002–1005 (2004).
17. G. Griffel, S. Arnold, D. Taskent, A. Serpengüzel, J. Connolly, and N. Morris, "Morphology-dependent resonances of a microsphere-optical fiber system," Opt. Lett. **21**, 695–697 (1996).
18. P. Bianucci, C. R. Fietz, J. W. Robertson, G. Shvets, and C.-K. Shih, "Whispering gallery mode microresonators as polarization converters," Opt. Lett. **32**, 2224–2226 (2007).
19. D. Goldstein, *Polarized Light* (Marcel Dekker, Inc., New York, 2003), 2nd ed.
20. M. J. Humphrey, E. Dale, A. T. Rosenberger, and D. K. Bandy, "Calculation of optimal fiber radius and whispering-gallery mode spectra for a fiber-coupled microsphere," Opt. Commun. **271**, 124–131 (2007).

1. Introduction

Whispering gallery mode (WGM) optical microcavities are widely known and used in many applications such as single molecule detection [1], nanoparticle sizing [2], compact narrow band filters [3], microlasers [4], optomechanical systems [5] and light switching [6]. Several materials are used in all these applications: Si, doped and undoped SiO_2, fluoride materials, III-V and II-VI semiconductors, polymers, chalcogenide glass, etc. WGM microcavities exist mostly in the form of microspheres [7], microdisks [4], microtoroids [8] and integrated ring resonators [9]. Main features of these microcavities include their high intrinsic quality factor (Q_0), their compactness and for some, their ease for on-chip integration.

Their optical characterization is usually done from their radiative emission spectrum collected by a free space setup or by measuring the transmission spectrum using the evanescent coupling to a waveguide. In the former case, the mode Q_0, related to the losses caused by scattering, absorption and radiative process, is directly obtained from the resonance peak full width half maximum (FWHM or $\Delta\lambda$). In the latter case, $\Delta\lambda$ is linked to the loaded or total quality factor ($Q_T = \lambda/\Delta\lambda$). It is related to Q_0 and the coupling quality factor Q_c by $Q_T^{-1} = Q_0^{-1} + Q_c^{-1}$. As the coupling is increased, the light tends to leave the cavity sooner via the waveguide, thus increasing the losses due to the coupling and decreasing Q_c. Depending on the dominating loss processes, the coupling regime can be identified as undercoupled ($Q_0 < Q_c$), critically coupled ($Q_0 = Q_c = 2Q_T$) or overcoupled ($Q_0 > Q_c$). Knowing precisely the contribution of the intrinsic losses and the coupling losses can be important in order to optimize the fabrication process or for pratical applications. For example, for sensing applications, the optimum sensitivity is achieved using a $Q_c = 2Q_0$ configuration [10]. In the case of filters or dispersion compensation devices, the maximization of Q_0 is desirable [11].

The simplest approach to measure Q_0 and Q_c is done by using Q_T and the normalized transmission value at the resonance wavelength λ_r [12]. Unfortunately, due to their symmetric contribution to Q_T, the coupling regime has to be known to distinguish between the Q_0 and Q_c contributions, except when critically coupled where the normalized transmission is zero. The coupling regime can be identified by varying the gap between the waveguide and the cavity. Since sensors or telecommuncations devices are mainly designed to be on-chip with fixed waveguide configuration, a correct determination can be difficult. Most Fabry-Perot characterization techniques cannot be used since a modulated signal in the frequency range of the free spectral range (FSR) is needed [13, 14]. Since WGM cavities usually have FSR above 100 GHz, instruments operating at these frequencies are not only very expensive, but they make the experimental setup bulky and cumbersome as well. Dumeige *et al.* [15] showed that Q_0 and Q_c extraction is possible if a laser line is swept fast enough across the resonance, because the

#154353 - $15.00 USD Received 12 Sep 2011; revised 13 Oct 2011; accepted 16 Oct 2011; published 3 Nov 2011
(C) 2011 OSA

resulting ringing phenomenom does not depend on Q_0 and Q_c in the same way. Unfortunately, this technique requires a high speed sweep and thus, cannot be applied to Q_T below 10^7. Finally, Ito *et al.* [16] also proposed a method limited to the case of two busline waveguides using the drop port and throughput port responses where both waveguides have the same coupling coefficient.

In this article, we propose a simple method to extract both Q_0 and Q_c and therefore the coupling regime of WGM and ring-type cavities. Based on a Stokes parameters analysis near the resonance wavelength, this single scan technique can be used to determine Q_0 and Q_c when Q_T is above 1×10^5 with $<1\%$ estimation error. Also, the method does not depend on the coupling regime nor on the input polarisation states. First, the theoretical model used to describe the Stokes parameters analysis is explained for different coupling regimes. The estimation of both quality factors is described with simple relations and the minimum Q_T where the technique is valid is determined based on the estimation errors. Then, we present the experimental setup and the measurements for different coupling gaps. The very good agreement of the experimental Stokes parameters curves supports the reliability of the proposed technique.

2. Theoretical model

The model used to extract Q_0 and Q_c is based on a polarization analysis (Stokes parameters) where the phase change in the WGM cavity gives, along with Q_T, an additional information about the coupling regime. In this section, we present the theoretical basis of how Q_0 and Q_c are determined and the conditions for which this technique is applicable.

The coupling arrangement is described in Fig. 1. An input polarization state $\vec{a}_x+\vec{a}_y=a_x\vec{x}+a_ye^{i\phi}\vec{y}$ enters the coupling region where a_x and a_y are the modulus of the x and y components, and ϕ, their phase difference. Only one axis is coupled to the cavity mode, we chose $\vec{a}_y$ in this article.

Thus, the x and y axes correspond to the quasi-TE and quasi-TM modes of the cavity. The coupled (κ^2) and uncoupled (t^2) power fractions are related to each other as $\kappa^2+t^2=1$ in the lossless case. They are related to Q_c by $Q_c=k_0n_mL/(1-t^2)$ [17], where $k_0=2\pi/\lambda$, n_m and L are the vacuum wavenumber, the mode refractive index and the round-trip path of the mode in the cavity respectively. The losses inside the cavity are described by the attenuation factor α via $\exp(-\alpha L)$. When the losses are small ($\exp(-\alpha L)\approx1-\alpha L$), α is related to the intrinsic

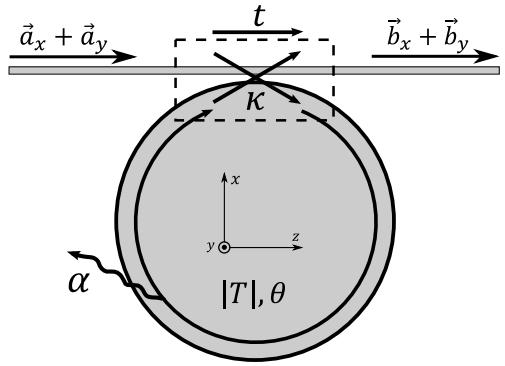

Fig. 1. Lossless coupling scheme between a single mode waveguide and an optical resonator. Polarization states $a_x\vec{x}+a_ye^{i\phi}\vec{y}$ and $b_x\vec{x}+b_y\vec{y}$ are entering and exiting the coupling region respectively. An amplitude transmission coefficient of $|T|$ and a phase difference of θ are added by the cavity. The power fraction $\kappa^2=1-t^2$ coupled to the cavity and the losses α characterize the waveguide-resonator system.

#154353 - $15.00 USD Received 12 Sep 2011; revised 13 Oct 2011; accepted 16 Oct 2011; published 3 Nov 2011
(C) 2011 OSA

quality factor by $Q_0 = k_0 n_m/(2\alpha)$. The exiting polarization state is described by $\vec{b}_x + \vec{b}_y$ and it can be expressed using a Jones matrices formulation [18]:

$$\begin{bmatrix} b_x \\ b_y \end{bmatrix} = \begin{bmatrix} 1 & 0 \\ 0 & |T|e^{i\theta} \end{bmatrix} \begin{bmatrix} a_x \\ a_y e^{i\phi} \end{bmatrix}.$$

We assume that the coupling region is lossless and the resonant frequencies of the TE/TM modes are sufficiently separated to leave $\vec{a}_x$ unperturbed by the cavity presence. If a mode were not sufficiently TE or TM, it would imply that $\vec{a}_x$ would be perturbed by the cavity response as well and this proposed model would no longer describe properly the polarization changes. We experimentally validated that the mode is quasi-TE(TM) by making sure that the measured resonance peak can be fully turned off (flat transmission) and back on by rotating the input linear polarization using the first half-wave plate HWP1 (see Fig. 3). The cavity's Jones matrix represents the complex response of a cavity mode coupled to a waveguide mode as follows [17]:

$$|T|^2 = \frac{t^2 + e^{-2\alpha L} - 2te^{-\alpha L}\cos(\beta_0 L)}{1 + t^2 e^{-2\alpha L} - 2te^{-\alpha L}\cos(\beta_0 L)} \tag{1}$$

$$\theta = \tan^{-1}\left(\frac{[t^2-1]e^{-\alpha L}\sin(\beta_0 L)}{t(1+e^{-2\alpha L}) - e^{-\alpha L}[1+t^2]\cos(\beta_0 L)}\right) \tag{2}$$

where $\beta_0 = k_0 n_m$, $|T|^2$ is the power transmission coefficient and θ is the phase change due to the interaction with the cavity. We assume the cavity is passive ($Q_0 > 0$) and that t, κ, ϕ and α are constant over the spectral range of interest, typically twice the FWHM.

The Stokes parameters can now be expressed in terms of the cavity parameters (T, θ) and the system parameters (a_x, a_y and ϕ) as follows [19]:

$$\begin{array}{ll} S_0 & = |b_x|^2 + |b_y|^2 = a_x^2 + |T|^2 a_y^2 \\ S_1 & = |b_x|^2 - |b_y|^2 = a_x^2 - |T|^2 a_y^2 \\ S_2 & = 2|b_x||b_y|\cos(\delta) = 2a_x a_y |T|\cos(\theta+\phi) \\ S_3 & = 2|b_x||b_y|\sin(\delta) = 2a_x a_y |T|\sin(\theta+\phi) \end{array} \tag{3}$$

where δ is the accumulated phase difference between axis. These expressions reveal that a spectral characterization of the Stokes parameters provides, along with the normalized transmission S_0, an additional information about the phase θ considering a non-zero value of a_x and a_y. Since S_0 and S_2 are similar to S_1 and S_3 respectively, the following equations are developed for S_2 but one can use S_3 as well since it only has a $\pi/2$ phase difference.

It is possible to represent S_2 as a function of the system parameters t, α, L, β_0 and ϕ by inserting Eq. (1) and Eq. (2) into the definition for S_2 using trigonometric identities:

$$S_2 = 2a_x a_y \frac{\cos(\phi)[t(1+e^{-2\alpha L}) - e^{-\alpha L}(1+t^2)\cos(\beta_0 L)] + \sin(\phi)e^{-\alpha L}(1-t^2)\sin(\beta_0 L)}{1 + t^2 e^{-2\alpha L} - 2te^{-\alpha L}\cos(\beta_0 L)}. \tag{4}$$

In Fig. 2, we present the Stokes parameters spectra calculated from Eq. (3) for different coupling regimes and different ϕ values. The spectra of S_0 in blue, S_1 in purple, S_2 in green and S_3 in red are shown for each case. It can be seen that the S_1 does not provide additional information compared to S_0 since it is only its complementary response.

The increasing amplitude of the S_2 and S_3 spectra as Q_c decreases can be understood considering that more photons are entering the cavity and are then recollected by the waveguide. Consequently, the polarization state of a higher amount of light is changed by the cavity. Since the S_0 spectrum tends to flatten as Q_c decreases, the S_2 spectrum can be used to spot collapsed peaks, mainly in the overcoupled regime (Fig. 2(e) and 2(f)).

#154353 - $15.00 USD Received 12 Sep 2011; revised 13 Oct 2011; accepted 16 Oct 2011; published 3 Nov 2011
(C) 2011 OSA

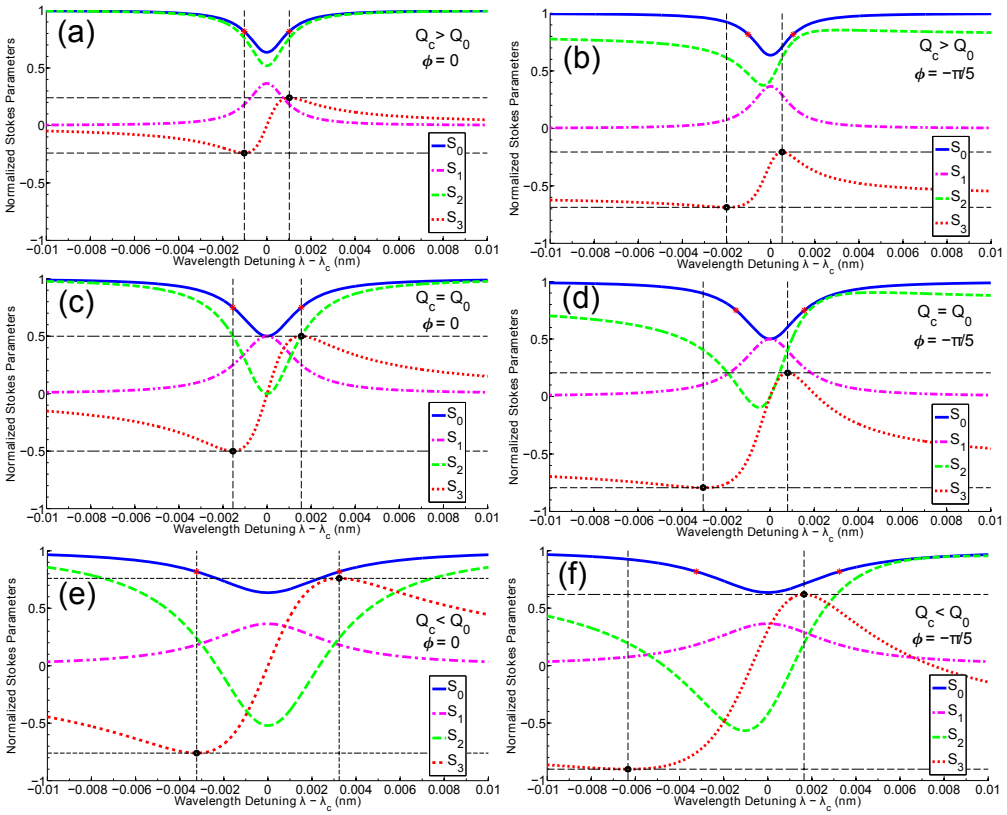

Fig. 2. Calculated spectra of the Stokes parameters across a resonance for the undercoupled regime 2(a)-2(b) ($Q_0 = 1\times10^6$ and $Q_c = 3\times10^6$), the critically coupled regime 2(c)-2(d) ($Q_0 = Q_c = 1\times10^6$) and the overcoupled regime 2(e)-2(f) ($Q_0 = 1\times10^6$ and $Q_c = 3\times10^5$). The case where $\phi = 0$ and $\phi = -\pi/5$ are shown on the left and right side respectively. The black and red dots represent the extrema of the S_3 spectra and the position of the FWHM values of S_0 respectively. a_x and a_y are set to $1/\sqrt{2}$.

The black dots indicate the extrema of the S_3 curves and the red dots show the points that define the FWHM of the S_0 curves. For $\phi = 0$, the wavelength positions of the black and red dots match for any coupling regime. In the case where $\phi \neq 0$, the positions no longer agree and the distance between black dots increases as the coupling increases. However, it can be seen that $\Delta S_2 = S_2^{max} - S_2^{min}$ and $\Delta S_3 = S_3^{max} - S_3^{min}$ do not change when ϕ is modified but increase monotonically when the coupling increases. Their values go from 0 to 1 as the coupling regime passes from undercoupled to critically coupled and from 1 to 2 as it passes from critically coupled to overcoupled. Compared to the resonance transmission value which can give the same value in the undercoupled regime and in overcoupled regime [12], ΔS_2 or ΔS_3 can be used to determine the coupling regime.

An additional feature of the S_3 spectrum (or S_2 spectrum depending on ϕ value) is its steep slope near the resonance, which is a consequence of its phase response dependency (Eq. (3)). This attribute can be exploited in applications where high sensitivity is required, such as biosensing or laser stabilization.

Using a normalized S_2 definition, $S_2^N = S_2/(2a_x a_y)$, it is possible to estimate Q_0 and Q_c. This

#154353 - $15.00 USD Received 12 Sep 2011; revised 13 Oct 2011; accepted 16 Oct 2011; published 3 Nov 2011
(C) 2011 OSA

can be done with S_3^N as well. The S_2 extrema are found by inserting their respective $\beta_0 L$ values, $\beta_0 L^{(1)}$ and $\beta_0 L^{(2)}$,

$$\beta_0 L^{(1)} = \arctan\left(\frac{-(1-t^2e^{-2\alpha L})\sin(\phi)}{\cos(\phi)(1+t^2e^{-2\alpha L})+2te^{-\alpha L}}\right)$$

$$\beta_0 L^{(2)} = \arctan\left(\frac{-(1-t^2e^{-2\alpha L})\sin(\phi)}{\cos(\phi)(1+t^2e^{-2\alpha L})-2te^{-\alpha L}}\right)+\pi$$

in Eq. (4). Using trigonometric identities, the resulting extrema, $S_2^{N,max}$ and $S_2^{N,min}$, are

$$S_2^{N,max} = \frac{S_2^{max}}{2a_x a_y} = \frac{t(1-e^{-2\alpha L})\cos(\phi)+e^{-\alpha L}(1-t^2)}{1-t^2e^{-2\alpha L}}$$

$$S_2^{N,min} = \frac{S_2^{min}}{2a_x a_y} = \frac{t(1-e^{-2\alpha L})\cos(\phi)-e^{-\alpha L}(1-t^2)}{1-t^2e^{-2\alpha L}}$$

where it can be seen that both have similar ϕ dependence. Thus, the difference $\Delta S_2^N = S_2^{N,max} - S_2^{N,min}$ can be written as:

$$\Delta S_2^N = \frac{\Delta S_2}{2a_x a_y} = \frac{2e^{-\alpha L}(1-t^2)}{1-t^2e^{-2\alpha L}} \approx \frac{2Q_0 - \beta_0 L}{Q_0 + Q_c - \beta_0 L} \tag{5}$$

using Q_0 and Q_c definitions and $\exp(-\alpha L) \approx 1-\alpha L$. This approximation represents a 0.5% deviation from the equality for $Q_0 > 10^4$, $\lambda \sim 1550$ nm, $n_m \sim 1.45$ and $L \sim 100\pi\ \mu$m.

Furthermore, the total quality factor Q_T quantifies the intrinsic and coupling optical losses as:

$$Q_T = \frac{\lambda}{\Delta\lambda} = \frac{Q_0 Q_c}{Q_0 + Q_c}. \tag{6}$$

Finally, both Q_0 and Q_c can be estimated from Eq. (5) and Eq. (6) as:

$$Q_0^{(e)} = \frac{4a_x a_y Q_T}{4a_x a_y - \Delta S_2} = \frac{2Q_T}{2-\Delta S_2^N} \text{ and } Q_c^{(e)} = 4a_x a_y \frac{Q_T}{\Delta S_2} = \frac{2Q_T}{\Delta S_2^N}$$

when $\beta_0 L$ can be neglected compared to Q_0 and Q_c. Thus, knowing a_x and a_y, both $Q_c^{(e)}$ and $Q_0^{(e)}$ can be extracted using a single measurement of $\Delta\lambda$ and ΔS_2. In order to be precise, these estimations require that the real Q_0 and Q_c be high enough. This condition is usually achieved for WGM and ring-type resonators. Also, since both are independent of ϕ, phase fluctuations do not change the results.

For a real measurement, however, we need to know within which limits these approximations hold based on a measurable quantity. We shall now define the lowest Q_T value needed in order to estimate Q_0 and Q_c within an acceptable error range. The relative errors of Q_c and Q_0, $\Delta Q_c/Q_c$ and $\Delta Q_0/Q_0$, are calculated from ΔS_2 and Q_T for each (Q_0, Q_c) combination, for Q_0 and Q_c above 10^4. We limit the analysis to 10^4 since previous assumptions (t, κ, α and ϕ constant) are not guaranteed below this limit. This lower value of Q_c implies a power coupling coefficient κ^2 up to 0.18 which includes realistic values below 0.05 or $Q_c > 3.7\times10^4$ for a WGM cavity-to-waveguide evanescent coupling [20]. Finally, we set $a_x = a_y = 1/\sqrt{2}$ where S_2 amplitude is maximized.

Using the calculations above, the relative errors in Q_0 and Q_c can be expressed as:

$$\frac{\Delta Q_0}{Q_0} = 1 - \frac{4a_x a_y Q_T}{(4a_x a_y - \Delta S_2)Q_0},$$

$$\frac{\Delta Q_c}{Q_c} = 1 - 4a_x a_y \frac{Q_T}{Q_c \Delta S_2}.$$

#154353 - $15.00 USD Received 12 Sep 2011; revised 13 Oct 2011; accepted 16 Oct 2011; published 3 Nov 2011
(C) 2011 OSA

For a relative error smaller than 1%, in the case of $Q_0^{(e)}$, it requires a $Q_0 \geq 10^4$ and a $Q_c \geq 10^5$. For $Q_c^{(e)}$, the combination (Q_0, Q_c) must be higher than $(1\times10^4, 7.5\times10^4)$ or $(9\times10^4, 1\times10^4)$. From Eq. (6), for a given Q_T value, Q_0 and Q_c are higher than Q_T. Consequently, the measured Q_T has to be above 10^5 in order to be within the 1% error limit of $Q_0^{(e)}$ and $Q_c^{(e)}$. For an error below 5%, a measured $Q_T \geq 2\times10^4$ is required.

3. Measurements and discussion

In order to relate the detected output signal of the cavity and the Stokes parameters, simple optical analysis can be used. The intensity of a signal passing through a wave plate with a dephasing angle of ϕ_l and a polarizer rotated of α_p compared to the wave plate axis is [19]:

$$I(\alpha_p, \phi_l) = \frac{1}{2}\left[S_0 + S_1\cos(2\alpha_p) + S_2\cos(\phi_l)\sin(2\alpha_p) + S_3\sin(\phi_l)\sin(2\alpha_p)\right].$$

The Stokes parameters can be related to different configurations of this optical system as follows:

$$\begin{aligned}
S_0 &= I(0^\circ,0^\circ) + I(90^\circ,0^\circ) \\
S_1 &= I(0^\circ,0^\circ) - I(90^\circ,0^\circ) \\
S_2 &= 2I(45^\circ,0^\circ) - I(0^\circ,0^\circ) - I(90^\circ,0^\circ) &&= 2I(45^\circ,0^\circ) - S_0 \\
S_3 &= 2I(45^\circ,90^\circ) - I(0^\circ,0^\circ) - I(90^\circ,0^\circ) &&= 2I(45^\circ,90^\circ) - S_0.
\end{aligned}$$

It should be noted that S_2 is easier to measure than S_3 since it does not need a quarter wave plate. S_0 and S_2 can be obtained by measuring the total power, $I(0^\circ,0^\circ) + I(90^\circ,0^\circ)$, and the intensity after the polarizer rotated by 45° with respect to the chosen reference axis, $I(45^\circ,0^\circ)$. The experimental setup used to simultaneously determine S_0 and S_2 is shown in Fig. 3. A tunable laser source (TLS) sweeps across the resonance wavelength while an oscilloscope (OSC) records the signal from the detectors D1 and D2. Both are synchronized via a trigger signal (TRIG). The first half wave plate HWP1 is used to rotate the linearly polarized output of the source and therefore, to control the input power ratio a_x^2/a_y^2. To ensure that the polarization state did not change along the SMF-28 fiber, the optical fiber length and curvature were minimized. Furthermore, before measurement and without any coupling to the cavity, the output polarization was measured after the collimator CO3 to ensure that it stayed linear along the fiber. To do so, a linear polarizer and a free space detector were used to verify the flatness of the polarization ellipse. We did not notice any significant change compared to the polarization ellipse measured

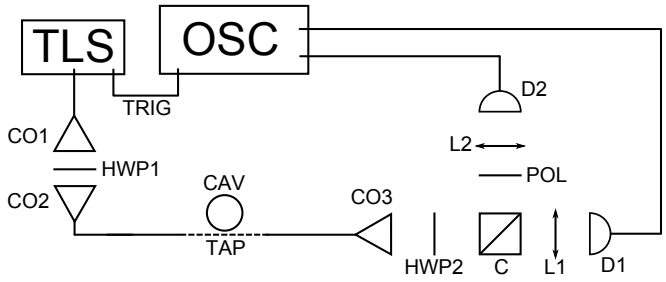

Fig. 3. Experimental setup used for S_0 and S_2 parameters measurements: TLS - Tunable laser source, OSC - Oscilloscope, TRIG - Trigger signal, CAV - Microcavity, TAP - Tapered fiber, C - 50:50 non-polarizing beamsplitter cube, CO1, CO2 et CO3 - Collimators, HWP1 et HWP2 - $\lambda/2$ wave plates, POL - Polarizer, L1 et L2 - Lens, D1 et D2 - Detectors. A SMF-28 fiber is used up to CO3.

#154353 - $15.00 USD Received 12 Sep 2011; revised 13 Oct 2011; accepted 16 Oct 2011; published 3 Nov 2011
(C) 2011 OSA

right after the collimator CO1. Thus, we conclude that the polarization along the optical fiber and the tapered fiber stays linear. The second half wave plate HWP2 is adjusted such as the x and y axis are turned 45° compared to the horizontal and vertical reference axis. This allows to write the detector intensities as a function of the cavity parameters in a simple form (Eq. (7)). Finally, the polarizer axis is set along the horizontal axis or 45° compared to a_x. Both signals are focused on the detectors. This simple configuration can be used to mesure the transmission spectrum via D1 without any modification. Since both signals are recorded simultaneously, any fluctuation in the resonance wavelength due to external parameters such as temperature does not affect the result.

A 1.2 μm diameter tapered optical fiber is used to couple the light to a silica toroidal microcavity. The microcavities are formed from a 0.8 μm thick thermal SiO_2 layer. Using a standard photolithographic process, the disk shapes are transfered to the silica layer. An SF_6 isotropic etch of the subjacent silicon follows. The toroidal shapes are obtained using laser reflow process [8]. The microtoroids have a 5 μm minor diameter and are formed out of a 100 μm diameter disk. A micrography of the coupling region is shown in Fig. 4. The gap between the tapered fiber and the cavity is controlled using a piezoelectric stage.

Using this experimental setup, the intensities detected at D1 and D2, I_1 and I_2, can be written as:

$$\begin{aligned} I_1 = &\quad |T_{45}|^2 a_x^2 + |T_{-45}|^2 |T|^2 a_y^2 \approx |T_{45}|^2 (a_x^2 + |T|^2 a_y^2) \\ I_2 \approx &\quad \tfrac{p_x^2 |R_{45}|^2}{2} \left[a_x^2 + |T|^2 a_y^2 + 2 a_x a_y |T| \cos(\theta + \phi) \right]. \end{aligned} \tag{7}$$

where the $|T_{45}|^2$ and $|T_{-45}|^2$ cube beamsplitter transmission coefficients are considered equal for a 45° and a $-45°$ linear input polarization with respect to the horizontal axis . The reflection coefficients, $|R_{45}|^2$ and $|R_{-45}|^2$, are also considered equal. p_x^2 is the polarizer transmission coefficient. Using these relations, the experimental normalized Stokes parameters $S_0^{N(e)}$ and $S_2^{N(e)}$ are retrieved as:

$$\begin{aligned} S_0^{N(e)} = &\quad \tfrac{I_1}{|T_{45}|^2 P_{tot}} = \tfrac{I_1}{I_1^{off}} \\ S_2^{N(e)} = &\quad \tfrac{\frac{2I_2}{p_x^2 |R_{45}|^2} - \frac{I_1}{|T_{45}|^2}}{2P_{tot}\sqrt{f(1-f)}} \end{aligned}$$

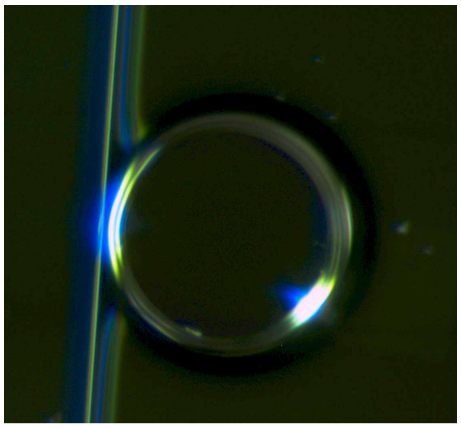

Fig. 4. Micrography of the resonator and waveguide. A 1.2 μm diameter tapered optical fiber is brought near to a toroidal silica microtoroid resonator using a piezoeletric stage.

#154353 - $15.00 USD Received 12 Sep 2011; revised 13 Oct 2011; accepted 16 Oct 2011; published 3 Nov 2011
(C) 2011 OSA

where f is the power fraction on the a_y axis. The total power, P_{tot}, is written as:

$$P_{tot} = a_x^2 + a_y^2 = \frac{I_1^{off}}{|T_{45}|^2} \rightarrow a_x = \sqrt{(1-f)P_{tot}} \text{ and } a_y = \sqrt{fP_{tot}}.$$

I_1^{off} is the intensity measurement at D1 off the resonance where the coupling can be neglected ($|T|^2 = 1$).

In Figs. 5(a)-5(c), the normalized $S_0^{N(e)}$ (red curve) and $S_2^{N(e)}$ (green curve) are shown for three coupling conditions (CC). The black dotted lines show the extrema of $S_2^{N(e)}$. The measured parameters, ΔS_2^N, Q_T and their corresponding $Q_0^{(e)}$ and $Q_c^{(e)}$ are presented in Table 1 for the three CC. The Q_T values were obtained by fitting a lorentzian curve to $S_0^{N(e)}$. This can be done

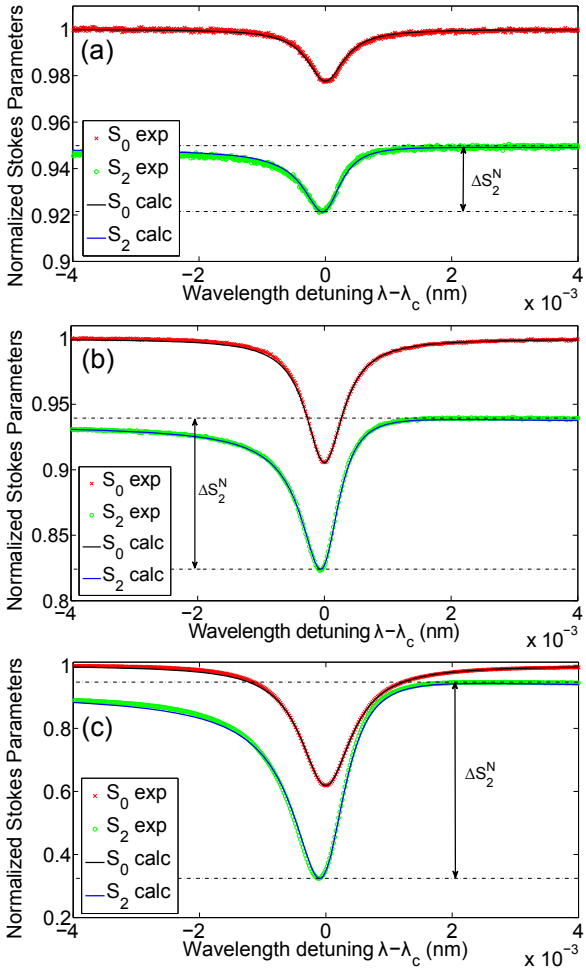

Fig. 5. Experimental and calculated S_0 and S_2 parameters obtained for three coupling conditions giving (a) $Q_0^{(e)} = (2.273 \pm 0.017) \times 10^6$ and $Q_c^{(e)} = (1.58 \pm 0.12) \times 10^8$ (b) $Q_0^{(e)} = (2.333 \pm 0.010) \times 10^6$ and $Q_c^{(e)} = (3.81 \pm 0.08) \times 10^7$ and (c) $Q_0^{(e)} = (2.311 \pm 0.009) \times 10^6$ and $Q_c^{(e)} = (5.11 \pm 0.03) \times 10^6$.

#154353 - $15.00 USD Received 12 Sep 2011; revised 13 Oct 2011; accepted 16 Oct 2011; published 3 Nov 2011
(C) 2011 OSA

because the FWHM and the center wavelength are the same for both S_0 and the transmission $|T|^2$. As it can be seen from the increasing amplitude of $S_2^{N(e)}$ from Fig. 5(a) to Fig. 5(c), the coupling coefficient is also increased, meaning a smaller gap betwen the waveguide and the cavity.

Using the extracted values of $Q_0^{(e)}$ and $Q_c^{(e)}$ in the proposed model (Eq. (1)-(3)), the calculated S_0 (black curve) and S_2 (blue curve) are drawn using f-parameters equal to 0.4, 0.435 and 0.445 for the first, second and third coupling condition respectively. These changes show the rotation of the polarization between different measurements. The ϕ parameter is extracted using the off resonance value of $S_2^{N(e)}$ where $\cos(\theta+\phi) \rightarrow \cos(\phi)$. There is a very good agreement between the experimental and the calculated curves, which shows that the proposed model, despite its simplicity, represents well the polarization changes inside the cavity.

Table 1. Extracted parameters from $S_0^{N(e)}$ (red curve) and $S_2^{N(e)}$ (green curve) presented in Fig. 5(a)-5(c).

CC	Q_T	ΔS_2^N	$Q_0^{(e)}$	$Q_c^{(e)}$
1	$(2.240 \pm 0.015) \times 10^6$	0.028 ± 0.002	$(2.273 \pm 0.017) \times 10^6$	$(1.58 \pm 0.12) \times 10^8$
2	$(2.198 \pm 0.007) \times 10^6$	0.115 ± 0.002	$(2.333 \pm 0.010) \times 10^6$	$(3.81 \pm 0.08) \times 10^7$
3	$(1.592 \pm 0.004) \times 10^6$	0.622 ± 0.002	$(2.311 \pm 0.009) \times 10^6$	$(5.11 \pm 0.03) \times 10^6$

It is worth noting the quasi constant value of $Q_0^{(e)}$ for the three coupling conditions. An additional measurement was taken for a very low coupling coefficient where $Q_T \approx Q_0$ gave a $Q_T = (2.26 \pm 0.05) \times 10^6$ which fits well with the presented data. This anticipated behavior shows that only the coupling losses are changed if the coupling conditions change. Thus, the intrinsic losses are only slightly changed by the fiber presence.

4. Conclusion

In this paper, we proposed a single scan method to quantitatively extract the intrinsic Q-factor Q_0 and the coupling Q-factor Q_c of a WGM or ring-type microcavity, regardless of the coupling regime. This technique is based on a simple Stokes parameters measurement. The theoretical model has been detailed and experimentally verified with a very good agreement. The determination of Q_0 and Q_c is accurate within 1 percent if Q_T is higher than 1×10^5. Compared to the laser sweeping technique [15] which is limited to $Q_T \sim 10^7$, our method can be used for lower Q_T resonators such as integrated microrings. The detection setup requires only simple optical components excluding usually needed fast electronics [13, 14]. This method provides a direct way to determine the relevant quality factors for waveguide-coupled microresonators, and is particularly useful for integrated systems.

Acknowledgements

We thank Dr. Bianucci, S. Virally and Dr. Saidi for useful discussions. This work was supported by the Natural Sciences and Engineering Research Council of Canada, Strategic Grant 365207-08 and the Fonds Québécois de la Recherche sur la Nature et les Technologies, Equip Grant PR-119043.

#154353 - $15.00 USD Received 12 Sep 2011; revised 13 Oct 2011; accepted 16 Oct 2011; published 3 Nov 2011
(C) 2011 OSA